Deposition loss of particles in the sampling lines of continuous emission monitoring system (CEMS) in coal-fired power plants

Runru Zhu[1], Yiyang Zhang[2*], Ye Yuan[3], Shuiqing Li[4]

[1] State Key Laboratory of Multiphase Complex Systems, Institute of Process Engineering, Chinese Academy of Sciences, Beijing 100190, China

[2]Key Laboratory of Advanced Reactor Engineering and Safety of Ministry of Education, Collaborative Innovation Center of Advanced Nuclear Energy Technology, Institute of Nuclear and New Energy Technology, Tsinghua University, Beijing 100084, China

[3]CFB Department, Huaneng Clean Energy Research Institute, Beijing 102209, China

[4]Key laboratory for Thermal Science and Power Engineering of Ministry of Education, Department of Thermal Engineering, Tsinghua University, Beijing 100084, China

Abstract

Facing the severe situation of air pollution, more stringent regulations of pollutant emissions are being promulgated in China, which calls for more accurate and reliable monitoring of particulate matter (PM) emission in coal-fired power plants. In this work we study the sampling loss of CEMS under different conditions by numerically solving particle transport equation in the sampling line. Featuring with a high Reynolds number, the particle deposition loss is severer than conventional laminar sampling and increases with Reynolds number when the plant load changes. The temperature difference between the hot sampling gas and pipe wall has a great effect on the sampling loss of PM 10. A small temperature difference of 2 K, which is very likely to exist even with a thick thermal insulation, will increase the deposition velocity of PM 1-2.5 by ten times. The surface roughness, either from pipe itself or deposited particles, also enhances the deposition loss by partly shifting the capture boundary to a higher diffusivity region. Combined all the possible factors, the loss ratio of 10 μm particles could reach 69% after 0.2 s and 95% after 0.5 s. The loss ratios of 2.5 and 1 μm particles are much lower, but also reach 4.1% and 7.9% respectively after 1 s, which cannot be neglected when a high accuracy monitoring is needed.

Keywords: deposition; CEMS; sampling; coal-fired power plant.

[*] Corresponding author. Tel: +86-10-62784824; Fax: +86-10-62797136

E-*mail address*: zhangyiyang@mail.tsinghua.edu.cn

INTRODUCTION

Although more stringent regulations of pollutant emissions have been promulgated, the fact of national-wide haze still indicate a severe air pollution situation in China (Zhang *et al.*, 2012; Gao et al., 2014; Liu *et al.*, 2014; Zheng *et al.*, 2017; Gao *et al.*, 2017). In 2016, among 338 major cities, only 84 cities met the air quality standard (Ministry of Environmental Protection of PRC, 2016), which means that the air quality of over 75% cities are still harmful to human health in a long-term view. The coal-fired power plants of China (Wang et al., 2016; Ma et al., 2017) that consume more than 50% coal per year, has been recognized as one of the major emission sources. The upgrade and transformation action plan for coal-fired power energy saving and emission reduction (2014–2020) which was released in 2014, required the emissions of particulate matter (PM) of coal-fired power plant to be under 10 mg/Nm^3(standard situation: 273K, 6% oxygen content). Though the regulation of PM emission is already quite strict even compared to developed countries, the accuracy of continuous emission monitoring system (CEMS) and gravimetric method (often used as the calibration for CEMS) could be the weak point, because the relative error may become larger for lower emission standard.

Installed at the flue-gas stack, the CEMS is mainly composed of a sampling line and a measuring device. A small portion of flue gas is extracted and measured by some on-line techniques, for example Beta attenuation or light scattering. Being different from gas phase

pollutants, the on-line measurement of PM is always disturbed by deposition loss along the sampling line. The loss ratio depends on various factors including particle size, flow rate, temperature difference etc., and sometimes could be quite large. However, the current specifications for continuous emissions monitoring of flue gas from stationary sources (HJ/T 75-2017 and HJ/T 76-2017) do not have requirements or guidelines on the sampling loss. Therefore, a detailed study is needed to address the issue of the sampling loss of CEMS under different conditions.

Compared with Beta attenuation, the light scattering technique has the advantage of convenience, safety and real-time response, thus widely adopted as the PM monitoring device in the coal-fired power plant CEMS in China. The typical flue gas velocity in the stack of power plants is around 20m/s. To keep an isokinetic condition and avoid blockage at the sampling nozzle, the flow rate of sampling gas is relatively large. Take the STACK-181WS type PM sensor system of PCME Ltd as an example, the nozzle diameter is 12 mm and the inner diameter of the sampling pipe is 20 mm. Considering of a sampling velocity of 25 m/s, the Reynolds number of the sample flow is about 7000, which has fully entered the turbulent regime. Comparing to conventional aerosol measuring instruments with laminar sampling flows (e.g. Electrical Low Pressure Impactor (ELPI), Re~1000), the highly turbulent flow in CEMS cause more deposition due to turbulent diffusion for small particles and inertia-eddy impaction for large

71 particles. Moreover, other factors, e.g. the temperature difference between flue gas and
72 environment, the roughness of sampling pipe surface, could further enhance particle deposition
73 along the sampling line.

74 The deposition of particles in a turbulent pipe flow is classical. In Lagrangian framework, by
75 using k-ε model, Large Eddy Simulation (LES) and Direct Numerical Simulation (DNS) to
76 determine the motion of fluid, the motion of particles was computed by Gosman & Ioannides
77 (1983), Wang & Squires (1996) and Ounis *et al.* (1993). However, the Lagrangian calculations
78 still face challenges when the number of the particles is important for investigation. For Eulerian
79 approach, the particle concentration problem can be easily handled by treating particle flow as a
80 fluid. Based on the remarkable contribution of Friedlander & Johnstone's (1957), the Eulerian
81 type calculation has been used in engineering solutions for a long time. By considering the
82 particle inertia and the inhomogeneity of fluid turbulent flow field in an area close to solid
83 surface, a new mechanism of particle transport which called turbophoresis is proposed by
84 Caporaloni *et al.* (1975) and Reeks (1983). Guha (1997) established a unified advection-diffusion
85 Eulerian theory, including molecular and turbulent diffusion, thermophoresis, turbophoresis,
86 shear-induced lift force, electrical forces, and gravity. Moreover, experimental results on particle
87 motion in turbulent flow are given by Shimada *et al.* (1993), Lee & Gieseke (1994), El-
88 Shobokshy (1983), Sehmel (1968) and Liu & Agarwal (1974), among others. The study of

89 particle transport loss in aerosol sampling line mostly focus on the urban environment aerosol
90 (Birmili *et al.*, 2007; Kumar *et al.*, 2008; Martuzevicius *et al.*, 2008; Kumar *et al.*, 2015). The
91 particle sampling loss of coal-fired power plant CEMS is more severe than conventional aerosol
92 measurements due to high Reynolds number of sampling flow, which has not been adequately
93 studied.

94 In this work we investigate the sampling loss in the CEMS of coal-fired power plants and
95 discuss various influencing factors. Special attention is paid to the practical conditions of CEMS
96 to reflect important parameters for different sized particles. The manuscript is organized as
97 following: Section II describes the numerical method; in Section III, the influences of Reynolds
98 number, temperature difference and pipe roughness on the particle deposition in the sampling line
99 are discussed; finally, we make an estimation on the loss ratio of difference sized particles and
100 the possible underestimation of CEMS.
101
102 **METHODS**
103
104 For describing physical process of particle deposition in the Eulerian framework，Guha (Guha,
105 1997; Guha, 2008) built a unified advection-diffusion theory by assuming particle phase as a
106 continuous fluid and then deriving this theory from the fundamental Eulerian conservation
107 equations of mass and momentum for the particles. For fully developed turbulence flow in a pipe,
108 this theory considered molecular and turbulent diffusion, thermophoresis, turbophoresis, gravity

and the drag force. For the boundary condition of the calculation domain, the effects of surface-roughness and particle interception are considered. Before we list the equations for this theory, note that the particle continuity equation for fully developed flow gives a constant particle mass flux in the particle deposition direction, because the particle phase is treated as continuous fluid.

For simplicity, the curvature of the sampling pipe is neglected for that the dimension is much larger than particle sizes (Guha, 1997). The geometry of the calculation is shown in Fig. 1. The particles deposition flux is given by

$$J = -\left(D_B + D_t\right)\frac{\partial c}{\partial y} - D_T c\frac{\partial \ln T}{\partial y} + cV_{py} \tag{1}$$

where

$$D_B = \frac{kT(1+2.7\mathrm{Kn})}{3\pi\mu d_p}$$

$$D_t = \varepsilon$$

$$D_T = D_B(1+\eta/kT)$$

where D_B, D_t and D_T are the Brownian diffusivity, turbulent diffusivity and the coefficient of temperature-gradient-dependent diffusion; c and J are the particle concentration and the flux of particles; y and V_{py} are the perpendicular distance from the wall and the particle mean velocity in this direction; T and η are the fluid temperature and the thermophoretic force coefficient; k, Kn, μ and d_p are the Boltzmann constant, Knudsen number, dynamic viscosity and the particle diameter; and ε is the eddy viscosity of the fluid. The particle deposition velocity V_{dep}, it is defined as $V_{dep}=J/c$. For the effect of gravitational settling, we have estimated that the terminal settling

velocities of 1, 2.5 and 10 μm particles are only 2.1%, 2.6% and 1.9% of the deposition velocities respectively under a typical condition in the sampling line. Hence the effect of gravitational settling is neglected in this study.

Eq. (1) can be numerically solved by combining the particle and the fluid motion equations together. The particle velocity can be derived from the particle momentum equations,

$$V_{py}\frac{\partial V_{py}}{\partial y}+\frac{V_{py}}{\tau_I}=-\frac{\partial V'^{2}_{py}}{\partial y} \tag{2}$$

$$V_{py}\frac{\partial V_{px}}{\partial y}=\frac{1}{\tau_I}\left(V_{fx}-V_{px}\right)+\left(1-\rho_f/\rho_p\right)g \tag{3}$$

where V_{px}, V'_{py} and V_{fx} are the particle mean velocity in the x direction, the particle RMS velocity and the fluid velocity in the x direction; ρ_f and τ_I are the fluid density and the inertial relaxation time.

The fluid motion is described as a function of the wall-coordinate y^+ ($y^+=y\times u_*/\upsilon$, where u_* and υ are the fluid slip velocity and the kinematic viscosity). And the functions are summarized in the Table 1.

To correlate fluid and particle Root Mean Square (RMS) motions, the following correlation is adopted (Binder & Hanratty, 1991).

$$V'^{2}_{py}=\Re V'^{2}_{fy}=\left[1+0.7\left(\tau_I/T_L\right)\right]^{-1}V'^{2}_{fy} \tag{4}$$

where $T_L=\varepsilon/V'_{fy}$ is the Lagrangian time scale. Using the non-dimensional form of u_*, υ, etc., Eq. (l)

and (2) can be normalized as following:

$$V_{dep}^{+} = -\left(\frac{D_B}{\nu} + \frac{D_t}{\nu}\right)\frac{\partial c^{+}}{\partial y^{+}} - D_T{}^{+}c^{+}\frac{\partial \ln T}{\partial y^{+}} + c^{+}V_{py}^{+} \tag{5}$$

$$V_{py}^{+}\frac{dV_{py}^{+}}{dy^{+}} + \frac{V_{py}^{+}}{\tau_I{}^{+}} = -\frac{d(V_{py}^{'+2})}{dy^{+}} \tag{6}$$

where

$$\begin{aligned} V_{dep}^{+} &= J / c_0 u_* \\ V_{py}^{+} &= V_{py} / u_* \\ c^{+} &= c / c_0 \\ V_{fy}^{'+} &= V_{fy}^{'} / u_* \\ D_T{}^{+} &= D_T / \nu \\ \tau^{+} &= \rho_p^0 d_p^2 u_*^2 \big/ \rho_f 18\nu^2 \end{aligned}$$

where V^{+}_{dep} and c_0 are the non-dimensional deposition rate and particle concentration at the centerline of the tube.

Two kinds of roughness will be considered in this work, the pipe surface roughness and the deposition roughness (illustrated in Fig. 1). The former one is the inherent rugged surface of the pipe, and the latter one is caused by deposited particles on the pipe surface. With a similar method as Grass (Grass, 1971) the starting point of the fluid velocity profile in pipe roughness cases is chosen as $0.55k_s$, where k_s is the effective roughness height. Under the effect of interception, the origin of the particle profile is $0.45k_s + d_p/2$. For the deposition roughness, we assume that $k_s = nl \times d_p$, where nl is the number of particle layers.

RESULTS AND DISCUSSION

161

162 ***Validation of the method***

163 Fig. 2 shows the comparison between calculation results and different experimental data in
164 literature. The horizontal axis is non-dimensional particle relaxation, and the vertical axis is non-
165 dimensional particle deposition velocity. The overall agreement is quite good, considering the
166 scattered distribution of the literature data. The deviation between the calculation and the
167 experimental data may due to the surface roughness difference. Three distinct regimes can be
168 identified by increasing particle relaxation time: turbulent diffusion regime, turbulent diffusion-
169 eddy impaction regime and particle inertia moderated regime. For practical sampling lines with a
170 typical Reynolds number of 6000, PM 2.5 ($\tau^+ \approx 0.58$, when d_p=2.5 μm) is mainly in the turbulent
171 diffusion regime and PM 10 ($\tau^+ \approx 9.2$, when d_p=10 μm) enters the turbulent diffusion-eddy
172 impaction.

173 The size range of discharging particles of coal-fired power plants of China is around 0.1~20
174 μm which locates in the turbulence diffusion and turbulent diffusion-eddy impaction regimes.
175 Electrostatic precipitator (ESP) is the most widely used major PM removal equipment in China,
176 and its particle penetration window is 0.1-1 μm (Liu *et al.*, 2016). On the other hand, in order to
177 meet the ultra-low emission standard of SO_2, wet flue gas desulfurization (WFGD) is also
178 equipped. At the outlet of the WFGD, the concentration of entrained droplet (solid content:
179 10%~20%) will be mainly reduced by inertial impaction (Zhang *et al.*, 2017) in the demisters.

According to the flue gas limestone/limegypsum desulfurization project technical specification (HJ/T 179 2018) and the datasheet of the commonly used demister (e.g. FLEXICHEVRON style VIII), the concentration of droplets at the demister outlet is 50 mg/m^3 with a cutoff diameter of 20 μm. Based on these two facts, we can estimate that the size range of particles in the sampling line of CEMS is about 0.1~20 μm.

The influence of Reynolds number

Fig. 3 shows the effect of Reynolds number (Re) on the deposition velocity of different sized particles. In practical conditions, the Reynolds number of the sampling flow varies with the power plant load because an isokinetic condition has to be maintained at the sampling nozzle. According to a typical sampling velocity of 10-30 m/s, the Reynolds number in the sampling line (inner diameter 10~30 mm) is within the range of 5000~15000 for different monitoring equipment (e.g. PCME STACK181WS, SDL SCS900PM and SICK FWE200DH). In Fig. 3, the flow considered are isothermal (ΔT=0K) and no roughness is assumed at the wall (k_s^+=0 and nl=0), in order to isolate the effect of Re. The results show that the effect of Re is quite different in different regimes. For small particles with short relaxation time, the deposition velocity increases nearly 3 times when Re increases from 6.4×10^3 to 1.5×10^4. In this diffusion-controlled regime, larger Re leads to larger turbulent diffusivity and thus significantly increases the deposition velocity. For larger particles entering the diffusion-eddy regime, the effect of Reynolds

number becomes much smaller as the contribution of eddy impaction overwhelms turbulent diffusion. As the particle relaxation time further increases to the inertia-moderated regime, the effect of Reynolds number again starts to emerge. For instance at a particle relaxation time τ^+ of 300 (corresponding to a size of larger than 10 μm), the deposition velocity increases by about 30% as the Reynolds number changes from 6.4×10^3 to 1.5×10^4, which shows that the influence of Reynolds number is less significant compared to the diffusion-controlled regime. The results indicate that the loss in the sampling line not only changes the total mass of particles but also changes the size distribution of the sampling aerosol which must be carefully accounted for. The deviation is larger for larger Reynolds number of sampling flow, especially for PM 2.5. Larger Reynolds number leads to larger turbulent diffusivity, which significantly increases the sampling loss of PM 2.5 in the diffusion-controlled regime. In such condition, the size distribution of CEMS will shift more to large particle size.

The influence of temperature difference ΔT

Due to the fouling and the corrosion problems, GGH is no longer a common equipment for coal-fired power plants in China. Therefore, the typical flue temperature of coal-fired power plants is around 60℃, significantly higher than the environment. Some of the new CEMS use heated sampling lines to eliminate the influence of the condensation. However, there are still many CEMS using non-heated sampling lines especially those use dilution sampling method.

And it should be noted that the heating of sampling line is not a mandatory term in the latest specifications yet. In such cases if the thermal insulation is not properly designed, the influence of thermophoresis will reveal and enhance particle loss in the sampling line. Fig. 4 shows the effect of temperature difference ΔT between the fluid and the wall on the deposition velocity. From Fig. 4(a), we can see that the influence of thermophoresis is quite remarkable even with a small temperature difference at the wall. The effect of thermophoresis is most significant to PM 2.5 in the diffusion-controlled regime, and rapidly drops as particle size increases. Fig. 4(b) shows the dimensionless ratio between particle thermophoretic velocity at y^+=0.3 and deposition velocity without thermophoresis. The ratio reaches a peak value of about 30 at τ^+=0.2 for all the temperature differences, which corresponds to a particle size of about 2 μm at Reynolds number of 6380. Even for a temperature difference as small as 1 K, the peak value of the ratio can be larger than 4, showing that thermophoresis largely enhances the deposition loss of PM 2.5 in the sampling line. We perform a simple heat transfer analysis considering the heat resistances of forced convection inside the pipe, conduction in the pipe wall and insulation, and natural convection outside the pipe. The result shows that if assuming the total temperature difference between the sampling flow and environment is 40 K, the temperature difference between the sampling flow and pipe wall is about 5 K when the pipe surface is bare and still larger than 3 K with 10 mm thick thermal insulation. The result suggests that the effect of thermophoresis must

234 be accounted for when evaluating the deposition loss along the piping line even with a thermal
235 insulation.

236 Moreover, the water vapor in the sampling gas may condense as flowing through the sampling
237 line if the line is not heated. The condensation on the particle surface could enlarge the size and
238 thus change the particle dynamics. Here we estimate the possible influence of this effect. With a
239 heat loss of 9.3 W/m, the mass of total vapor condensation after 2m sampling line is about 7.9
240 g/Nm^3. On the other hand, it should be noted that the area of pipe inner surface is over 16000
241 times larger than the total surface area of air-borne particles, which indicates that most vapor
242 condenses on the pipe surface. Only a very small fraction of vapor condensation occurs on the
243 particle surface, which is about 0.47 mg/ Nm^3. This quantity of condensation only enlarges the
244 particle size by about 1.6%. Hence, we ignore the effect of vapor condensation on particle
245 dynamics in this study. For other situations e.g. an even larger heat loss, the effect of vapor
246 condensation could be significant and needs to be considered.

247 ***The influence of roughness***

248 *Pipe roughness*

249 Fig. 5(a) shows the variation of deposition velocity with relaxation time for three different
250 effective roughness heights. The tendency of the calculation agrees well with the experimental
251 data in literature. It should be noted that the real roughness of sampling pipe is usually 0~0.5 for

252 plastic pipes and 0.5-1.5 for steel pipes. For PM 10, larger roughness leads to larger deposition
253 velocity. For even larger particles in the inertia-moderated regime, the effect of surface roughness
254 is minor. Fig. 5(b) explains the reason why surface roughness enhances particle deposition in the
255 sampling pipe. The turbulent diffusivity increases with y^+ in the boundary layer. Therefore, with
256 k_s^+ increase from 0.5 to 1.5, the D_t/ν increases by about 10 times, which indicates that the tips of
257 roughnesses have reached to a region of larger turbulent diffusivity and local particles are more
258 likely to be captured by these roughnesses. Since turbulent diffusion is an important deposition
259 mechansim for PM 10 in the sampling line, the effect of surface roughness needs to be considered.
260 *Deposition roughness*
261 Besides natural roughness of pipe inner surface, the accumulation of deposited particles also
262 produces another type of roughness, here named as 'deposition roughness'. The critical pull-off
263 force derived from the Johnson-Kendall-Roberts (JKR) theory is equal to $1.5\pi wR$, where R is the
264 effective radius between particles and wall, and its value is $d_p/2$; w is the work of adhesion with
265 typical values about 10-30mJ/m^2 (Liu et al., 2016). The value of critical pull-off force is about 10^{-8}-10^{-7} N for micro-sized particles. And the drag force act on the particles located in the viscous
267 sublayer is about 10^{-10}-10^{-9} N. The comparison between critical pull-off force and drag force
268 indicates that the re-suspension is not likely to occur in the viscous sublayer and thus the
269 deposited particles will act in a similar way as natural roughness. In this work, we treat the effect

of deposited roughness the same as the pipe roughness, as illustrated in Fig. 1. The enhancement of deposition velocity due to deposition roughness is shown in Fig. 6. Different from the influence of pipe roughness, deposited roughness mainly affects the turbulent diffusion-eddy impaction regime, corresponding to size range 1~10 μm. Similar to the pipe roughness, the deposition velocity increases with the number of deposited paritcle layer. If starting from a brand-new sampling pipe, the accumulation of deposited particles on the inner surface will accelerate the deposition process, which forms a positive feedback until the deposits grow out of the viscous sublayer and re-suspend by the flow drag. We can make a rough estimation on the time needed to form a layer of particles (e.g. *nl*=1). Assuming a particle concentration of 10 mg/Nm^3 with 44% PM 10+, the time to reach 50% coverage is less than 7h. The real situation is more complicated that the deposition roughness of large particles also enhances the deposition of small particles. Therefore, the effect of deposition roughness needs to be carefully considered.

Underestimation of PM emission due to sampling loss

Based on the above discussions, we can estimate the deposition loss in a sampling line in a CEMS. The loss ratio *LR* is deduced from particle deposition velocity,

$$LR = 1 - \exp\left(-4V_{dep}t_r / D\right) \quad (7)$$

where t_r is the residence time of particle in the sampling line, and *D* is the inner diameter of the sampling pipe, taken as 10 mm.

Fig. 7(a) shows the loss ratio increasing with the residence time. The dashed lines are the basic cases at Reynolds number 6380, without considering any temperature difference, pipe roughness or deposition roughness. The solid lines are the cases of Reynolds number 8680 (ΔRe=2300), temperature difference ΔT=5 K, pipe roughness k_s^+=1, and deposited particle layer nl=1. As shown by the dashed lines, the loss ratio of 10 μm particles reaches 60% after a residence time of 1.0 s while the loss ratios of 1 and 2.5 μm particles are both below 0.1%, if no temperature difference or roughness is considered. With all these effects properly accounted, the solid lines indicate that the loss ratio of 10 μm particles is nearly 1 and the loss ratios of 1 and 2.5 μm particles increase to 4.1% and 7.9% respectively. Fig 7(b) shows the contribution of each effect. We can see that for 1 and 2.5 μm particle, the major increases result from the effects of temperature difference (~50 times) and pipe roughness (~25 times) while the effects of Reynolds number and deposition roughness are relatively minor. For 10 μm particle, the influences of all the four factors are close. The results suggest that the sampling loss of large particles (~10 μm) must be considered because a major portion of air-borne particles may deposit along the sampling line and cause a large deviation of CEMS. The loss of PM 2.5 should also be concerned especially when there is a large temperature difference or surface roughness.

Based on the above analysis, we can make a rough estimation on the total amount of PM that is underestimated due to the sampling loss in CEMS. For simplicity, the size of 1, 2.5 and 10 μm are

306 chosen to represent the loss ratio of PM 2.5, PM 2.5~10, and PM 10+ respectively. Measurements
307 by ELPI show that the mass fractions (*mf*) of PM 2.5, PM 2.5~10 and PM 10+ are about 42.7%,
308 13.3% and 44% respectively (Zhao *et al.*, 2016). The total underestimation per standard flue gas
309 due to sampling loss is given by,

310
$$m_e = ES \times mf_{PM2.5} \times LR_{PM2.5} + ES \times mf_{PM2.5\sim10} \times LR_{PM2.5\sim10} + ES \times mf_{PM10+} \times LR_{PM10+} \quad (8)$$

311 where *ES* is the emission standard, $LR_{PM2.5}$, $LR_{PM2.5\sim10}$ and LR_{PM10+} are the loss ratio of PM2.5,
312 PM2.5~10 and PM10+ respectively. We use 10 mg/Nm^3 (ultra-low emission) as the emission
313 standard, and the residence time is 0.5 s. Calculation results indicate that the underestimation of
314 the CEMS could be 4.3 mg/Nm^3 with most contribution from PM 10+.

315

316 **CONCLUSIONS**

317

318 In this work we investigate the deposition loss along the sampling line of continuous emission
319 monitoring system (CEMS) in coal-fired power plants. The deposition velocities of different
320 sized particles under various conditions are obtained by solving particle transport equation in a
321 turbulent pipe flow. The loss ratio that could affect the accuracy of CEMS is then calculated for
322 different conditions. The main conclusions are as following:

323 1) For the typical Reynolds number of sampling flow in CEMS, the main deposition
324 mechanisms for PM2.5, PM2.5-10, PM10+ are turbulent diffusion, turbulent diffusion-eddy

impaction, and inertia impaction. To keep an isokinetic condition at the sampling nozzle, the Reynolds number in the sampling line may vary in the range of 5000-15000 depending on the power plant load. Increasing Reynolds number leads to larger deposition velocity in the turbulent diffusion and inertia moderated regimes but shows little effect in the turbulent diffusion-eddy impaction regime;

2) The contribution of thermophoresis on the deposition loss is quite significant for PM 10. With a temperature difference as small as 2 K, which is very likely to exist even with a thick thermal insulation, the deposition velocity of PM 1-2.5 will increase by ten times. This suggests that in order to obtain an accurate monitoring of PM 10 emission, the temperature of the pipe wall needs to be equal to or higher than the sampling gas in CEMS;

3) The surface roughness, either from pipe itself or deposited particles, will enhance the deposition loss by partly shifting the capture boundary to a higher diffusivity region. The influence of pipe roughness is most profound for PM 10 particles, which could be as large as 50 times with a common roughness of 20 μm. This effect needs to be particularly considered for the start-up stage of CEMS ;

4) Combined all the possible factors, the loss ratio of 10 μm particles could reach 69% after 0.2 s residence time and 95% after 0.5 s residence time. The loss ratios of 2.5 and 1 μm particles are

much lower, but also reach 4.1% and 7.9% respectively after 1 s residence time, which can not be neglected if a high accuracy monitoring is expected.

ACKNOWLEDGMENTS

This work was supported by National Natural Science Funds of China (No. 51776109), Tsinghua University Scientific Research Fund (No. 20151080381) and National S&T Major Project (No. ZX069). And Runru Zhu wish to thank Dr. Ye Zhuang for his valuable advices.

REFERENCES

Binder, J.L. and Hanratty, T.J. (1991). A diffusion model for droplet deposition in gas/liquid annular flow. *Int. J. Multiph. Flow* 17:1–11

Birmili, W., Stopfkuchen, K., Hermann, M., Wiedensohler, A. and Heintzenberg, J. (2007). Particle penetration through a 300m inlet pipe for sampling atmospheric aerosols from a tall meteorological tower. *Aerosol sci. tech.* 41:811-817.

Caporaloni, M., Tampieri F., Trombetti, F. and Vittori, O. (1975). Transport of particles in nonisotropic air turbulence. *J. Atmos. Sci*. 32:565–68

El-Shobokshy, M.S. (1983). Experimental measurements of aerosol deposition to smooth and rough surfaces. *Atmos. Environ.* 17:639-644.

362 Friedlander, S.K. and Johnstone, H.F. (1957). Deposition of suspended particles from turbulent
363 gas streams. *Ind. Eng. Chem.* 49: 1151-1156.
364 Gao, L., Zhang, R., Han, Z., Fu, C., Yan, P., Wang, T., Hong, S. and Jiao, L. (2014). A modeling
365 study of a typical winter PM2.5 pollution episode in a city in eastern China. *Aerosol Air*
366 *Qual. Res.* 14: 311–322.
367 Gao, Q., Li, S.Q., Yang, M.M., Biswas, P. and Yao, Q. (2017). Measurement and numerical
368 simulation of ultrafine particle size distribution in the early stage of high-sodium lignite
369 combustion. *Proc. Combust. Inst.* 36: 2083-2090.
370 Gosman, A.D. and Ioannides, E. (1983). Aspects of computer simulation of liquid-fueled
371 combustors. *J. Energy* 7: 482–490.
372 Grass, A.J. (1971). Structural features of turbulent flow over smooth and rough boundaries. *J.*
373 *Fluid Mech.* 50: 233–255.
374 Guha, A. (1997). A unified eulerian theory of turbulent deposition to smooth and rough surfaces.
375 *J. Aerosol Sci.* 28:1517-1537.
376 Guha, A. (2008). Transport and deposition of particles in turbulent and laminar flow. *Annu. Rev.*
377 *Fluid Mech.* 40: 311–341.
378 Kumar, A., Gupta, T. (2015). Development and laboratory performance evaluation of a variable
379 configuration PM1/PM2.5 impaction-based sampler. *Aerosol Air Qual. Res.* 15: 768–775.
380 Kumar, P., Fennell, P., Symonds, J. and Britter, R. (2008). Treatment of losses of ultrafine aerosol

particles in long sampling tubes during ambient measurements. *Atmos. Environ.* 42: 8819–8826.

Lee, K.W. and Gieseke, J.A. (1994). Deposition of particles in turbulent pipe flows. *J. Aerosol Sci.* 25: 699-709.

Liu, B.Y.H. and Ilori, T.A. (1974). Aerosol deposition in turbulent pipe flow. *Environ. Sci. Technol.* 8: 351-356.

Liu, W.W., Li, S.Q. and Chen, S. (2016). Computer simulation of random loose packings of micro-particles in presence of adhesion and friction. *Powder Technol.* 302: 414–422.

Liu, X.W., Xu, Y.S., Fan, B., Lv, C., Xu, M.H., Pan, S.W., Zhang, K., Li, L. and Gao, X.P. (2016). Field Measurements on the Emission and Removal of PM2.5 from Coal-Fired Power Stations: 2. Studies on two 135 MW circulating fluidized bed boilers respectively equipped with an electrostatic precipitator and a hybrid electrostatic filter precipitator. *Energy Fuels* 30: 5922−5929.

Liu, Y.J., Zhang, T.T., Liu, Q.Y., Zhang, R.J., Sun, Z.Q. and Zhang, M.G. (2014). Seasonal variation of physical and chemical properties in TSP, PM10 and PM2.5 at a roadside site in Beijing and their influence on atmospheric visibility. *Aerosol Air Qual. Res.* 14: 954–969.

Ma, Z.Z., Li, Z., Jiang, J.K., Deng, J.G., Zhao, Y., Wang, S.X., Duan, L. (2017). PM2.5 emission reduction by technical improvement in a typical coal-fired power plant in China. *Aerosol Air*

399 *Qual. Res.* 17: 636–643.

400 Martuzevicius, D., Grinshpun, S.A., Lee, T., Hu, S.H., Biswas, P., Reponen, T. and LeMasters G.

401 (2008). Traffic-related PM2.5 aerosol in residential houses located near major highways:

402 indoor versus outdoor concentrations. *Atmos. Environ.* 42: 6575–6585.

403 Ministry of Environmental Protection of PRC (2016). China Environmental Status Bulletin 2016.

404 Ministry of Environmental Protection of PRC (2017). Specifications for continuous emissions of

405 SO_2, NO_X, and particulate matter in the flue gas emitted form stationary sources. HJ 75-2017.

406 Ministry of Environmental Protection of PRC (2017). Specifications and test procedures for

407 continuous emission monitoring system for SO_2, NO_X, and particulate matter in flue gas

408 emitted form stationary sources. HJ 76-2017.

409 Ministry of Environmental Protection of PRC (2018). General technical specification of flue gas

410 limestone/lime-gypsum wet desulfurization. HJ 179-2018.

411 Ounis, H., Ahmadi, G. and McLaughlin, J.B. (1993). Brownian particle deposition in a directly

412 simulated turbulent channel flow. *Phys. Fluids* 5:1427–1432

413 Postma, A.K. and Schwendiman, L.C. (1960). Studies in micrometrics: I. Particle deposition in

414 conduits as a source of error in aerosol sampling. Report HW-65308, Richland, Washington:

415 Hanford Laboratory.

416 Reeks M.W. (1983). The transport of discrete particles in inhomogeneous turbulence. *J. Aerosol*

417 *Sci.* 14:729–739

418 Sehmel, G.A. (1968) Aerosol deposition from turbulent airstreams in vertical conduits. Report
419 BNWL-578, Richland, Washington: Pacific Northwest Laboratory.

420 Shimada, M., Okuyama, K. and Asai, M. (1993) Deposition of submicron aerosol particles in
421 turbulent and transitional flow. *AIChE J.* 39:17-26.

422 Wang, Q. and Squires, K.D. (1996). Large eddy simulation of particle-laden turbulent channel
423 flow. *Phys. Fluids* 8:1207–1223.

424 Wang, Y., Cheng, K., Tian, H.Z., Yi, P., Xue Z.G. (2016). PM2.5 Emission characteristics and
425 control prospects of primary PM2.5 from fossil fuel power plants in China. Aerosol Air Qual.
426 Res. 16: 3290-3301.

427 Wells, A.C. (1967). Chamberlain, Transport of small particles to vertical surfaces. *Br. J. Appl.*
428 *Phys.* 18:1793-1799.

429 Zhang, H., Li, Y.Z., Li, J.X. and Liu, Q.F. (2017). Study on separation abilities of moisture
430 separators based on droplet collision models. *Nucl. Eng. Des.* 325: 135–148.

431 Zhang, R.J., Tao, J., Ho, K.F., Shen, Z.X., Wang, G.H., Cao, J.J., Liu, S.X., Zhang, L.M. and Lee,
432 S.C. (2012). Characterization of atmospheric organic and elemental carbon of PM2.5 in a
433 typical semi-arid area of northeastern China. *Aerosol Air Qual. Res.* 12: 792–802.

434 Zhao, L. and Zhou, H.G. (2016). Particle removal efficiency analysis of WESP in an ultra-low

435 emission coal-fired power plant. *Proceedings of the CSEE* 36:468-473 (in Chinese).

436 Zheng, C.H., Shen J.L., Zhang, Y.X., Zhu, X.B., Wu, X.C., Chen, L.H. and Gao, X. (2017).

437 Atmospheric emission characteristics and control policies of anthropogenic VOCs from

438 industrial sources in Yangtze river delta region, China. *Aerosol Air Qual. Res.* 17: 2263–2275.

439

440 **Table 1.** Fluid motion functions.

Parameter	Functions	
Mean motion of the, fluid in the x direction, V_{fx}	$V_{fx} = u_* y^+$	$y^+ \le 5$
	$V_{fx} = u_*(-1.706 + 1.445 y^+ - 0.04885 y^{+2} + 0.0005813 y^{+3}$	$5 < y^+ < 30$
	$V_{fx} = u_*\left(2.5 \ln y^+ + 5.5\right)$	$y^+ > 30$
Fluid RMS velocity in the y direction, V'_{fy}	$\left(\overline{V}'_{fy}\right)^2 = 0.005 y^{+4} u_*^2 / \left(1 + 0.002923 y^{+2.218}\right)^2$	
Temperature profile of the fluid, T	$T = \frac{\Pr y^+}{\Delta T^+_{200}} \Delta T + T_W$	$y^+ < 5$
	$T = \frac{5\Pr + 5\ln\left(0.2\Pr y^+ + 1 - \Pr\right)}{\Delta T^+_{200}} \Delta T + T_W$	$5 \le y^+ \le 30$
	$T = \frac{5\Pr + 5\ln\left(1 + 5\Pr\right) + 2.5\ln\left(y^+ / 30\right)}{\Delta T^+_{200}} \Delta T + T_W$	$30 \le y^+ \le 200$
	where Pr is the Prandtl number, ΔT is the temperature difference between y^+=200 and the wall and T_W is the wall temperature.	
Eddy viscosity of the fluid, ε	$\varepsilon = \upsilon y^{+\left(4 - y^{+0.08}\right)} \left[\frac{2.5 \times 10^7}{\mathrm{Re}}\right]^{\left(-y^+/(400+y^+)\right)} \times 10^{-3}$	
	where Re is the Reynold number based on the average fluid velocity.	

441

442

443 **Figure Captions**

444 **Fig. 1.** Illustration of the particle deposition process.

445 **Fig. 2.** Comparison of calculation and experimental data on particle deposition.

446 **Fig. 3.** The dimensionless deposition velocity profile with different Re. (k_s^+=0, ΔT=0K, nl=0)

447 **Fig. 4.** The influence of temperature difference. (a)The dimensionless deposition velocity profile

448 with different ΔT; (b) the $V^+_{Tdep}/\ V^+_{dep(\Delta T=0K)}$ profile. (k_s^+=0, Re=6.4×10^3, nl=0)

449 **Fig. 5.** The influence of pipe roughness. (a)The dimensionless deposition velocity profile with

450 different effective roughness height; (b) Variation of the turbulent diffusivity in the y-direction.

451 (ΔT=0, Re=6.4×10^3, nl=0)

452 **Fig. 6.** The dimensionless deposition velocity profile with different particles layer number （Δ

453 T=0K, Re=6.4×10^3）

454 **Fig. 7.** Variation of the loss ratio for different diameter particles. (a) the particle loss ratio due to

455 increase in residence time. (b) the average loss ratio of different deposition mechanism.

456

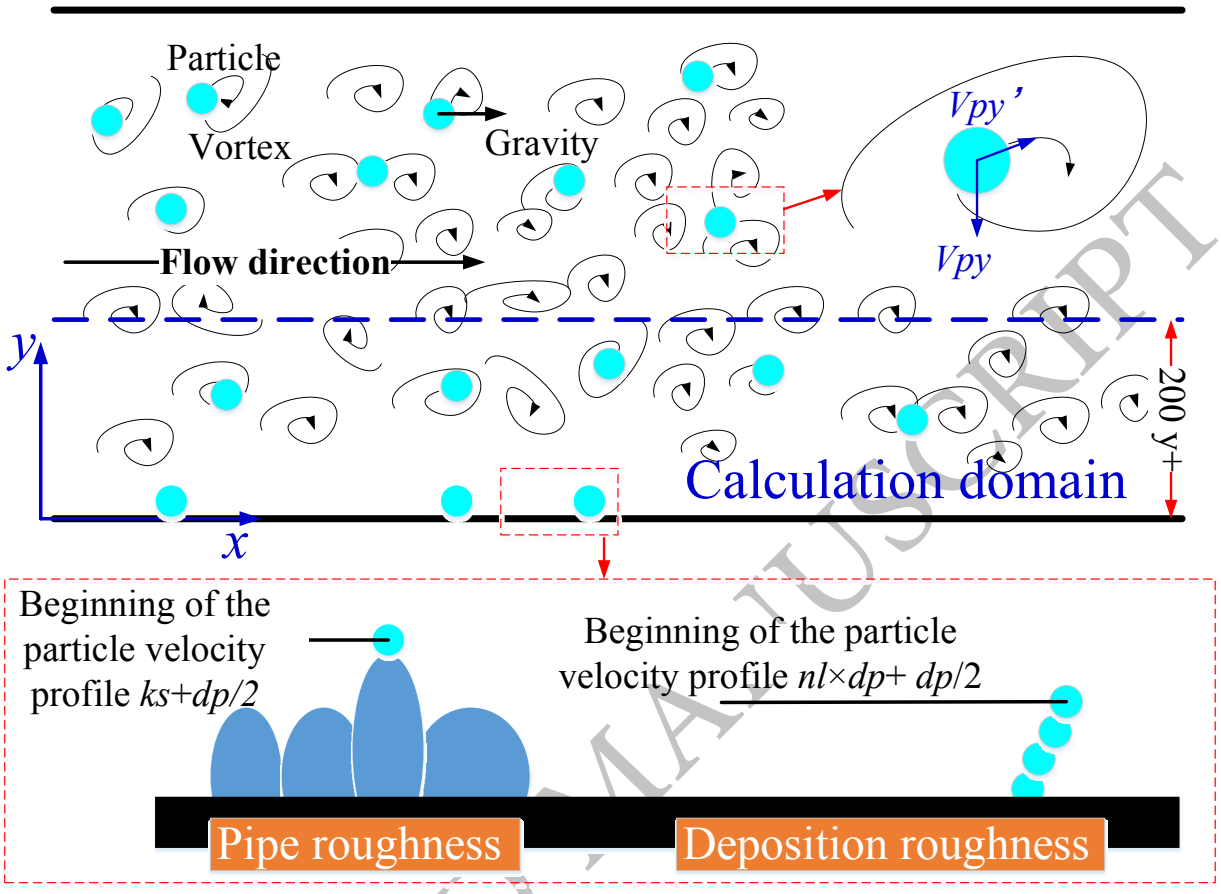

Fig. 1.

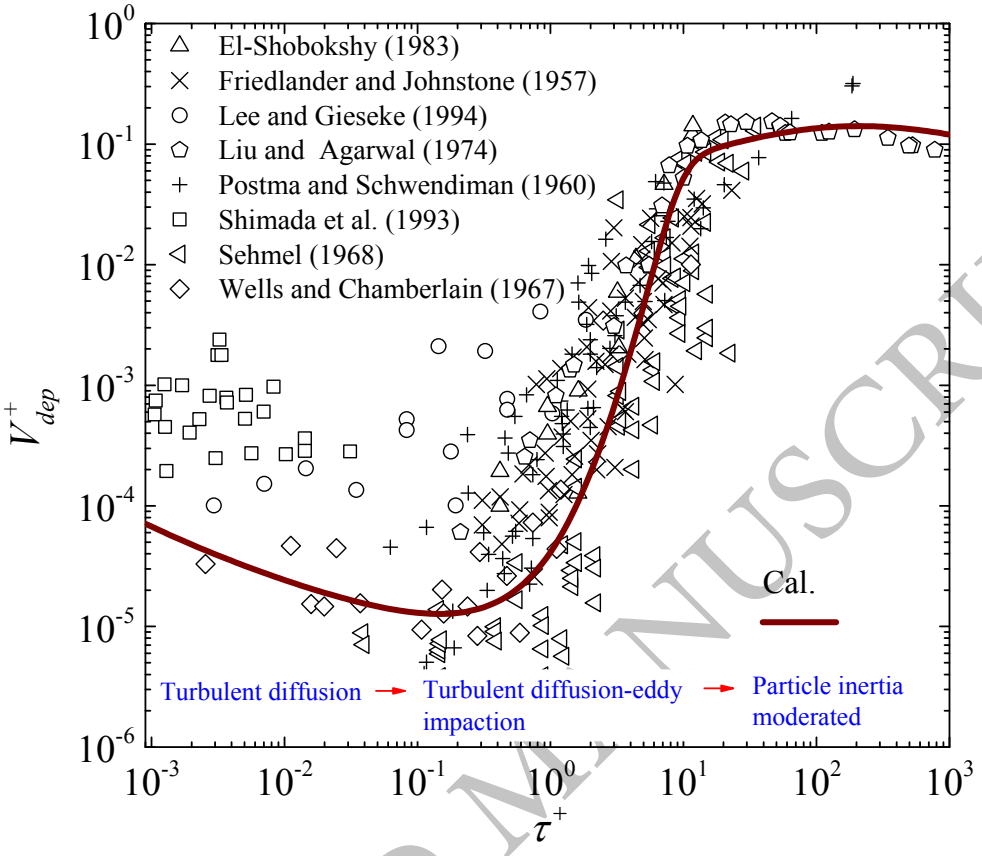

461

462 **Fig. 2.**

463

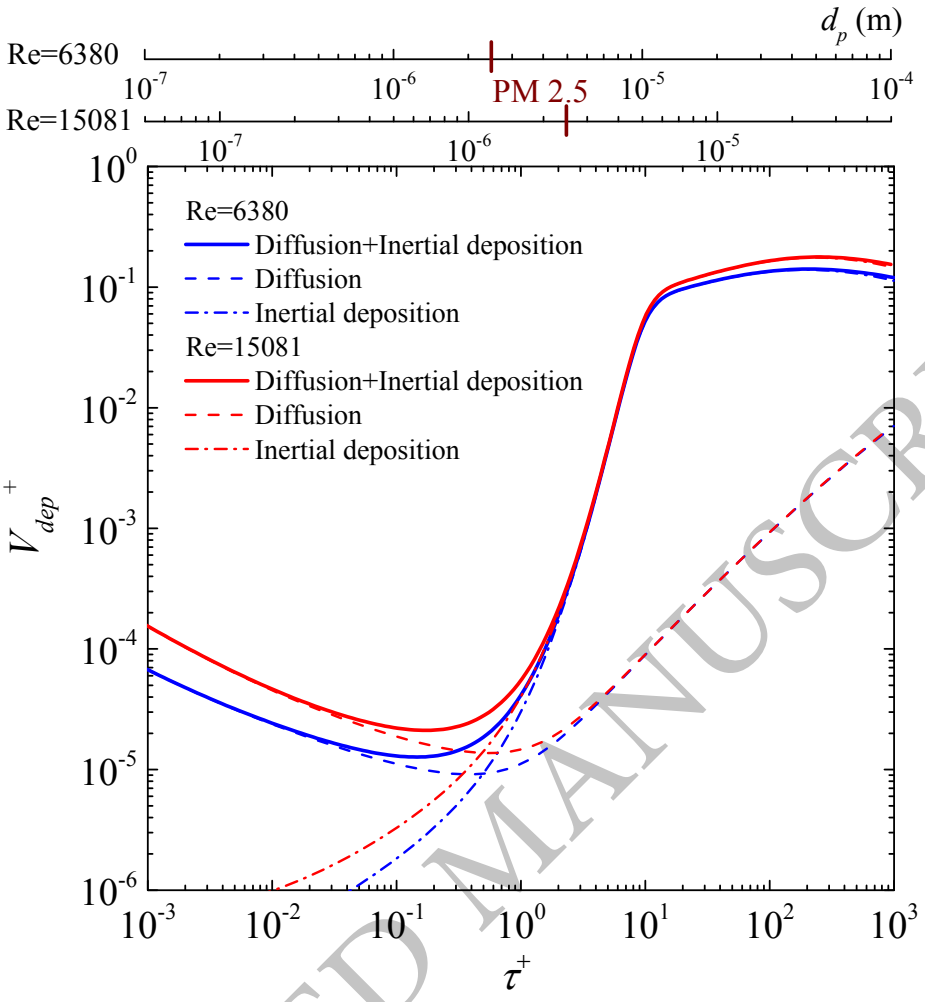

464

465 **Fig. 3.**

466

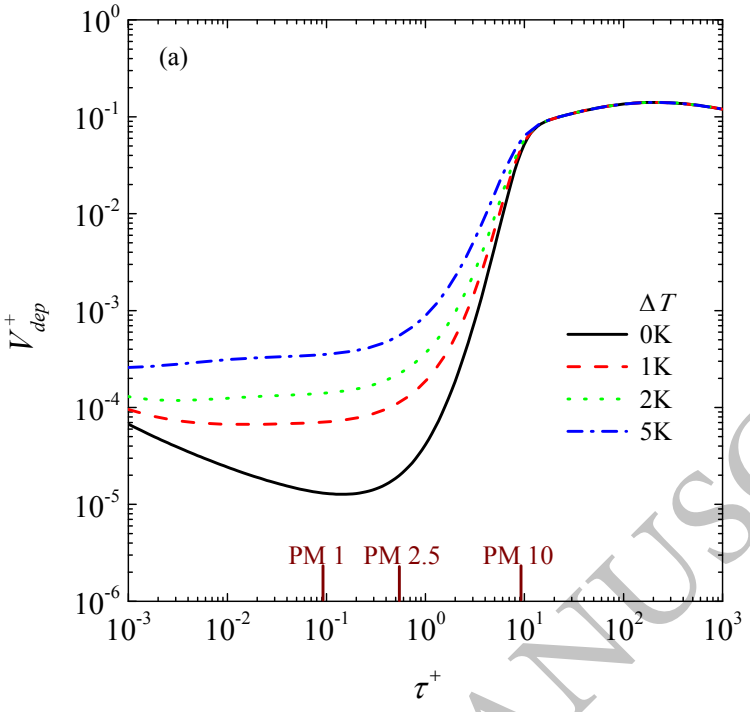

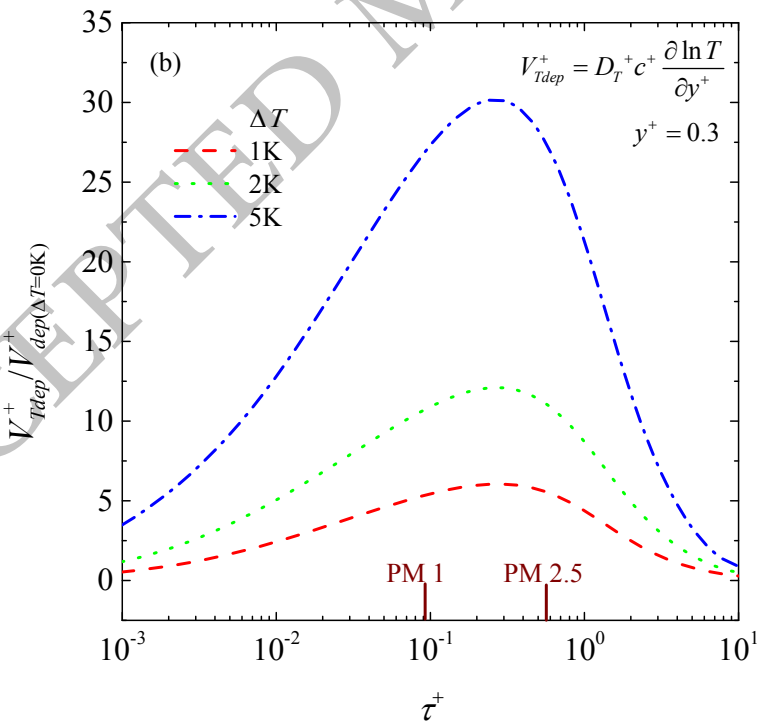

Fig. 4.

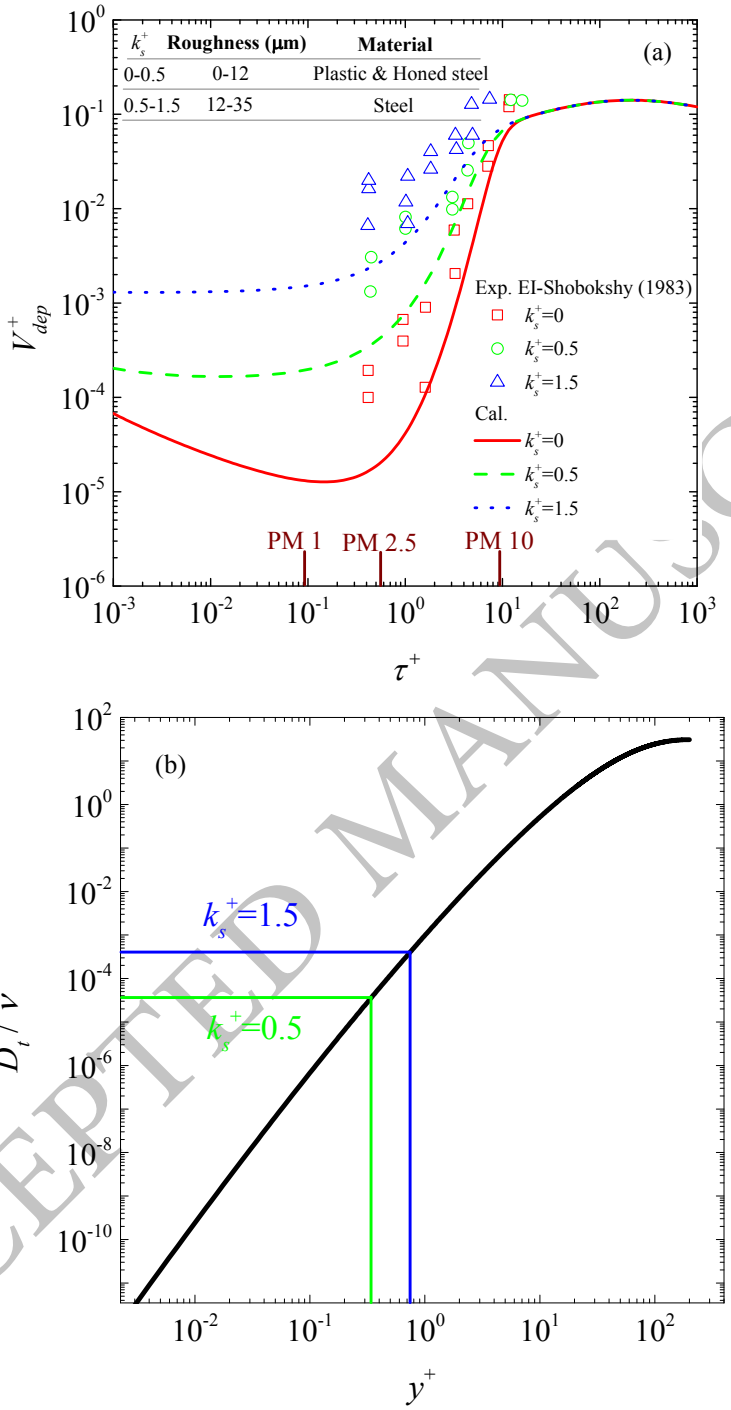

Fig. 5.

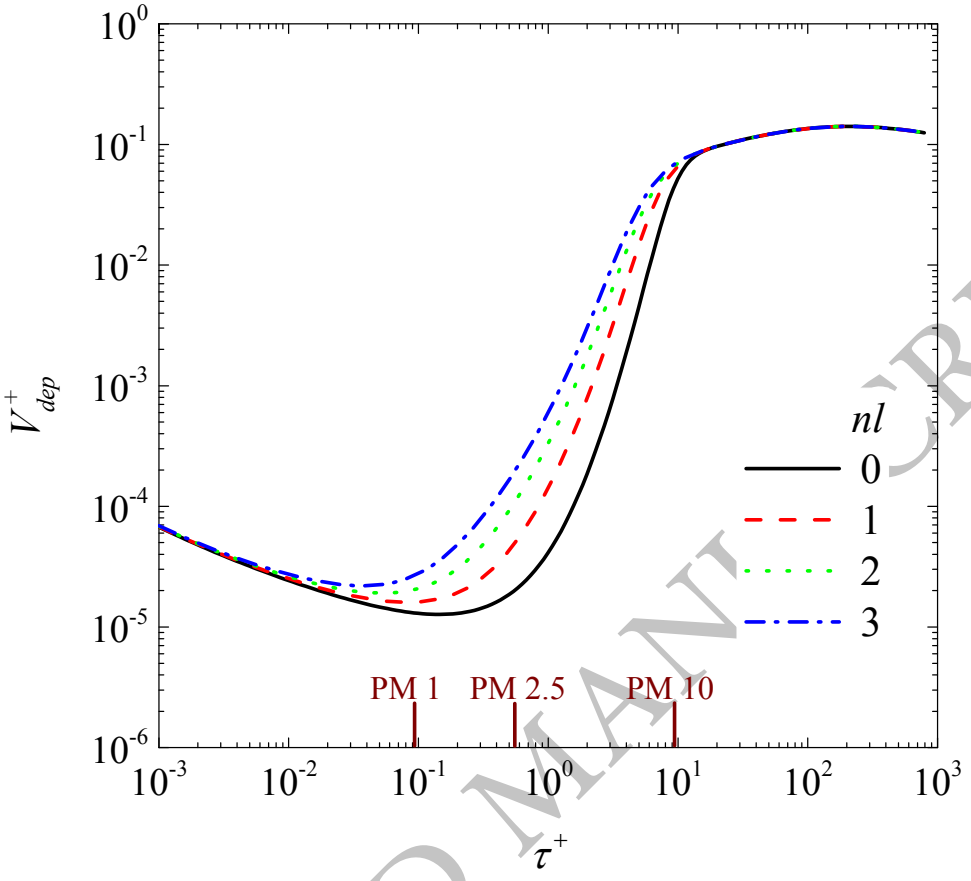

475

476 **Fig. 6.**

477

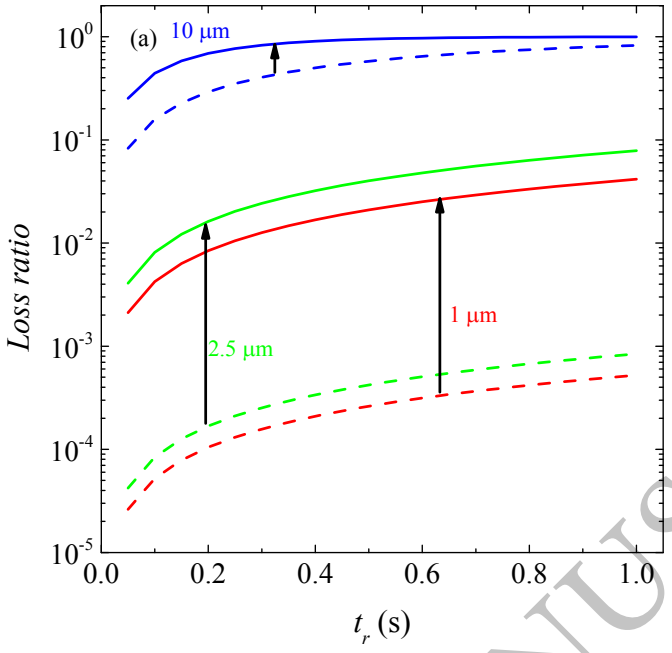

478

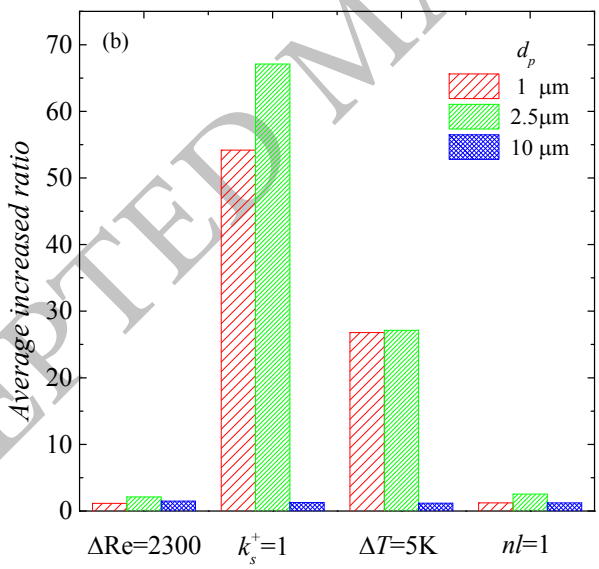

479

480 **Fig. 7.**